Coordination Chemistry Reviews, 125 (1993) 231–240

Local probe microscopies and their applications to semiconducting materials

O. Enea

Laboratoire de Chimie 4, URA 350, Université de Poitiers
40, avenue du Recteur Pineau, 86000 Poitiers, France.

Abstract

The aim of this work is two-fold: -to describe the principles of scanning tunneling (STM) and scanning force (SFM) microscopies; -to summarize the most important results obtained so far on atom-resolved surfaces of Si or GaAs and from the study of photocatalysts like TiO_2 (single crystals, powders, fractal electrodes, transparent ceramics).

INTRODUCTION

The discovery of local probe microscopies in the last decade was a considerable advance with respect to the optical or electron microscopies, limited by the wavelength of the beam and/or the aberrations of the lens system.

Beside the remarkable high resolution attained in Scanning Tunneling (STM) or Scanning Force (SFM or AFM) microscopies there are several other important advantages:

- to obtain direct information about the various features (domains and active sites such as defaults, steps, deposits,...) and the distribution of the total charge density or the charge density waves (CDW) on the surface;

-to operate not only under ultrahigh vacuum (UHV) conditions, but also in air, in solvents and even in electrolytes with samples submitted to potentiostatic sequences;

-to follow in real time the dynamics of various processes such as the transformation of domains, the dissolution or crystallisation of minerals, the rearrangement of biological molecules, etc.

-to manipulate and to modify on a nanometer scale the surface of materials.

The application of local probe microscopies to metallurgy, electronics, bioengineering, catalysis, electrochemistry or photochemistry has great interest and this accounts for the exponential growth of the number of publications since the discovery of STM.

The goal of this review is to summarize, after a short presentation of the basic principles of local probe microscopies, the most important up-to-date information pertaining to semiconducting materials.

0010-8545/93/$24.00

1. PRINCIPLES

1.1. Probes and interactions

The image of a microscopic object (or part thereof) can be obtained by scanning a local probe which probes a local property of the object or produces a local, reversible or irreversible modification via some interaction between probe and object. A probe can be the apex of a sharp metallic tip (STM), a tip mounted on a flexible arm (SFM), etc.

Interactions used for imaging include a) tunneling current, b) forces, c) capacitance, etc,...

a) The tunneling current occurs when a sharp metallic tip ending with a few atoms is scanned at only a few angströms over the surface of an electrically conducting sample submitted to a small bias voltage ranging from a few millivolts to a few volts. The tip probes the local density of states and the tunneling current is a measure of the overlap of tip wave functions with the sample wave functions.

b) Attractive or repulsive forces, the nature and magnitude of which can vary considerably with the distance, occur when the tip mounted on a cantilever spring is scanned like a profilometer on the surface of a conductive, semiconductive or insulator sample. At large distances, attractive forces such as electrostatic or van der Waals forces dominate, while at very small distances repulsive forces prevail.

c) As a capacitance probe, a tip allows capacitance imaging in the 10 nm range. The capacitance is of the order of a 10^{-18} Farad and can be measured with an accuracy of about 10^{-22} Farad either via the Coulomb force or with a classical capacitance measuring circuit.

1.2. Scanning Tunneling Microscopy (STM)

The tunneling current depends exponentially on the separation (s) between probe tip and sample: $I_t = B \cdot \exp(-AF^{1/2} \cdot s)$. Due to the exponential relationship between I_t and s, a high vertical resolution (up to 0.02Å) can be reached, the real limit being the stability of the distance probe-object electronically controlled through the feedback current. The lateral resolution L depends not only on the size of the probe (radius R) but also on the local properties of the sample. There are no simple general resolution criteria, but in a first approximation, the lateral resolution depends on (R+s) and ranges between 1 and 2 Å.

1.2.1. Operating modes

The data collection is generally performed in one of two ways:

-**constant current mode**: The tip is moved along a fixed trajectory in the x direction, and the tunneling current I_t monitored. A feedback loop is then used to move the tip up or down in order to maintain a constant current. At the end of a single scan, the tip is displaced a single step in the y direction, and the scan repeated ; the image obtained is thus a linescan plot of (x, y, z);

-**constant height mode**: The tip-sample distance s is set during the scan, and the variation in tunneling current is plotted as a function of the lateral position. Only very flat areas of the sample can be scanned, but the imaging speed can be increased by a factor of up to two orders of magnitude with respect to the constant current mode. Linescan plots obtained either in constant height or constant current mode are further transformed by image processing computers into grey-scale or colour images.

1.2.2. Imaging modes

-Topographic mode: Different images but closely reflecting the same topography or geometrical structure of the sample can be obtained by following either z(x,y) (constant current operation mode) or I_t(x,y) (constant height operation mode) as variable, provided the interaction itself and the response of the object to it are homogeneous.

However, STM images strongly depend on tunneling conditions since fixing I_t as a reference current and V at a given bias voltage will determine the gap distance s, and thus the feature which can be seen on the surface.

The atomically resolved images obtained in the case of semiconductors are often strongly dependent on the sample-tip bias voltage in a nontrivial manner. It is therefore important to try several positive and negative voltages and to compare the images reflecting the topography through the distribution of surface states.

When a voltage V is applied to the sample, its energy levels will be rigidly shifted upwards or downwards energy by the amount $|eV|$, depending on whether the polarity is negative or positive, respectively.

For any given lateral position of the tip above the sample, the tunneling current I_t is determined by the sample-tip separation (s), the applied voltage (V), and the electronic structure of the sample and tip, which is quantitavely described by their respective density of states.

-Spectroscopic mode: A quantitative information regarding the spatial localization of electronic states is obtained by using modulation techniques to measure dI_t/dV (at s = constant or I_t = constant) as a function of V, usually referred to as "Scanning Tunneling Spectroscopy" or STS.

Voltage-dependent STM imaging is the simplest way of obtaining spectroscopic information, by acquiring conventional STM "topographic" information at different applied voltages and comparing the results.

More complete information can be obtained over a wider energy range simultaneously from complete I_t-V measurements, at the expense of considerably more complicated data acquisition electronics and data handling.

1.3. Scanning Force (or Atomic Force) Microscopy (SFM, AFM)

The tip (Si_3N_4) is either in direct constant with the sample (repulsive mode), or maintained above the sample (attractive mode), but in both cases, the sample is moved rather than the delicate tip mount.

The exact approach employed in SFM depends upon whether the attractive or repulsive forces between tip and sample are to be probed. In both attractive and repulsive SFM, the tip is mounted on a cantilever spring, with the amplitude or frequency of the spring deflection being used to obtain the surface topography as the tip is rastered across the surface.

Profiling is achieved by moving the sample up or down during a scan to maintain a constant vibration amplitude: the image is then simply a contour map of (x, y, z).

The imaging modes used in SFM are: -the topographic mode, using a constant force (ranging from 10^{-9} to 10^{-11} Newtons) and measuring changes of height (s); -the spectroscopic mode in which the height s is kept constant and the force is measured.

Atomic resolution can be achieved in SFM, but the vertical resolution is less good than in STM because the inverse power low dependence of force on distance is less sensitive to variations in s as the exponentially depending tunnel current.

2. APPLICATIONS TO SEMICONDUCTING MATERIALS

2.1. Fundamental information on atom-resolved surfaces

While most physical methods and particularly diffraction techniques usually provide statistically averaged data, STM (or SFM) offers the possibility of obtaining atomically resolved information on real structures without long-range order. For example, statistically distributed atomic defects can be resolved, domain boundaries, dislocations, and locally ordered (or disordered) parts of the surface observed, the atomic structure of steps and terraces analyzed, and the cleanliness of the sample surface estimated. Besides, since the tunneling of the electrons is determined by the local density of states, STM may be used to find local chemical effects, metal-like behavior, maxima or minima band gaps, etc...

Both STM and SFM can be used, but the interpretation of atom-resolved images requires great care because STM is directly sensitive to the charge modulation of the conduction electrons (i.e. to CDW), whereas SFM responds only to the atomic surface structure [1] [2]. The STM and SFM images of a same sample might be very different as in the case of $TaSe_2$ [1], or very similar, as in the case of HOPG [2], but showing different types of atomic sites.

2.1.1. Well defined surfaces of Si, GaAs, and InP

Transitions from ordered to disordered surface structures have been examined [3] on the atomic scale by STM on laser- and thermally annealed Si(111). Highly disordered surface areas show many missing adatoms leaving two-dimensionally "isolated" silicon atoms with in-plane nearest-neighbour distances greater than 10Å.

STM was also applied to the real-time observation of the heating-current-induced step motion (the so called "electromigration effect") on the Si(111) surface at temperatures between 1100 and 1142 K near the (1x1)-(7x7) phase transition [4]. The steps were found to shift in the opposite direction to the heating current direction or to the electric field. This behavior is explained by a simple model of the existence of positively charged Si adatoms on the (1x1) domains together with pinning centers for the step shifting such as impurities, adsorbates or local stresses.

Domain boundaries on Si(111))-(7x7) surface run in a zig-zag pattern, which causes terraces to be reconstructed [5].

The initial stage of the (1x1)-(7x7) phase transition of the Si(111) surface occurs around 1140 K and their fluctuations were observed in real-time by STM [6]. As the temperature decreases the disordered (1x1) phase disappears and the surface undergoes a reversible phase transition to the ordered (7x7) phase, the most stable at room temperature.

The real shapes of the (7x7) domains are equilateral triangles which are surrounded by unfaulted triangles. There is a critical size around 6 units of (7x7), smaller domains are so unstable that they disappear rapidly [6].

Triangular facets extending over large areas of a few thousands Å but with a height of a single atomic layer were observed by STM [7] on the surface of cleaved GaAs (110). The steps occur along the [001], the [112] and in a few cases the [114] direction, leading to a repetitive pattern of triangular structures.

The investigation of the GaAs (110) at various voltages reveals [8] that the topography observed by STM in UHV conditions undergoes structural changes as function of the applied bias voltage. For positive bias voltages, the unoccupied (Ga-derived) states are probed while for negative voltages the occupied (As-derived) states are observed. The corrugation manifests itself in rows along two directions

(001 and 110), due to the strong localization of the implied surface bonds: dangling and back bonds.

Several different vicinal GaAs (001) surfaces, grown by molecular beam epitaxy (MBE) were imaged by STM [9] and the effects of different growth conditions directly observed. The temperature increase influences the thermodynamic distribution of terrace width as well as the straightness of the step edges. Growth by migration enhanced epitaxy is likely to improve the incorporation at step edge kink sites, and to improve the step quality.

High levels of Si doping of MBE-grown GaAs (001) induce a change in the ordering of the (2x4)/c(2x8) surface reconstruction [10]. A large number of kinks forming domain boundaries between well ordered regions of c(2x8) surface is seen on STM images. Each kink site can accept one electron and allow electrons in the doped layer to drop from the Fermi level to the acceptor state, lowering the electronic energy of the surface region. The band-bending that results from this causes pinning of the Fermi level at the surface.

The electronic structure of InP(110) surface and the spatial distribution of the surface states was investigated by scanning tunneling microscopy and spectroscopy [11]. Atome-resolved images were simultaneously obtained for the occupied and the empty surface states localized at the P and the In atoms, respectively, to determine their relative position within the unit cell.

2.1.2. Hydrogen-induced reconstructions

The making and the breaking of Si-H bonds is rate determining in technologically important processes such as chemical-vapor deposition, reactive ion-etching, etc. The chemistry of hydrogen on the Si(100) surface was studied by STM at various temperatures and H coverages [12]. The (2x1) and (3x1) surfaces are well ordered and stable in the presence of atomic hydrogen while the (1x1) structure is poorly ordered and liable to spontaneous etching by hydrogen atoms. The repulsive steric interaction between dihydride units on (1x1) surface weakens the Si-H bonds and stabilizes the (3x1) surface observed at 400 K. While the tilted dihydride surface is found to be energetically favored at high hydrogen coverage, the reduced interaction between the hydrogen atoms on this surface occurs at the expense of increased strain in the Si-Si back bonds.

2.1.3. Oxygen-induced reconstructions

The oxidation of silicon is perhaps the most important chemical reaction in the field of microelectronic materials, and the nature of the bonding site of oxygen in the early stages of oxidation has been the subject of extensive studies [13]. STM, atom-resolved STS, and electronic structure calculation were used to determine the nature of the adsorption state of oxygen in the initial stages of the oxidation of Si(111). Two states of adsorbed oxygen were imaged: one of them was identified as a Si adatom site with one oxygen atom inserted in one of the back bonds, while the other involves an oxygen atom tying up the adatom dangling bond with another oxygen atom inserted in one of the back bonds. As the coverage is increased towards the monolayer, the latter site becomes the dominant one.

A fast STM system was used for the real-time observation of the initial stages of oxygen interaction with Si(100)-(2x1) at room temperature [14]. Numerous atomic processes were identified: -the formation of bridges between rows of dimers leading to an antiphase buckling in both rows over a length of 100 Å, -disappearance of complete dimers leading to the formation of holes,

-apparition, between dimers, of protruding features on the scale of a (2x1) unit cell, etc...

In contrast to the Si(111)-(7x7) surface which has a metallic density of states (DOS), the dangling bonds of the Si dimers on the (2x1) surface are paired, leading to the formation of a surface gap and a vanishing DOS near E_F. By using STM and STS to study the initial stages of oxidation of the Si(100)-(2x1) surface, it was possible to observe a reduced reactivity of Si dimers towards O_2 compared to that of Si adatoms on Si(111)-(7x7). Defects on the Si(100)-(2x1) surface which have a metallic DOS dominate the reactivity towards O_2 in the early stages of the reaction.

Bumps (1.4 Å high) generated on top of the surface by the exposure to O_2 form elongated islands upon annealing. Bumps and islands appear to be due to silicon ejected to the surface by the oxidation process.

Only 53 % of the areas having no defects are oxidized upon exposure to layers of oxygen [16]. Single steps seem to be quite stable against oxidation.

Information on both the rate and progression of the native oxide growth over 100 x 100 nm^2 areas of the semiconductor surfaces, was provided by STM study of the nature of oxides on the GaAs(100) and InP(100) chemically etched surfaces. On both semiconductor surfaces the oxide growth was observed to proceed via nucleation centres dispersed across the surface which eventually coalesced to form a uniform oxide layer approximately 2 nm thick. The rate of oxide growth on the GaAs etched surface was found to be significantly faster than on the InP surface.

2.1.4. Adsorbate-induced reconstructions

Since single atoms may be identified by means of STM, the nature of critical nuclei and their adsorption sites can be determined. This kind of information is important to solve the problem of heteroepitaxy, which plays a dominant role in the future development of semiconductor devices.

Typical examples for metal-reconstructions of the silicon (111) surface are those occurring for In or Ga deposition [17]. Depending on the amount of metal coverage (ranging from the clean substrate to one monolayer ML), In/Si(111) is reconstructed in several phases as follows:

$$(7x7) \rightarrow (\sqrt{3}x\sqrt{3}) \rightarrow (\sqrt{31}x\sqrt{31}) \rightarrow (\sqrt{7}x\sqrt{3}) \rightarrow (4x1) \rightarrow (1x1)$$

and a similar sequence is observed for Ga/Si(111). Ga behaves like In at low coverages (up to 1/3 ML): Ga atoms replace Si in the (7x7) positions, preserving the (7x7) structure. At 1/3 ML, Ga induces a $(\sqrt{3}x\sqrt{3})$ reconstruction identical to that of In and Al on Si(111). When the coverage is increased to 1/2 ML, Ga induces totally different reconstructions from those induced by In.

In the STM experiments on the low-coverage (less than 1/3 ML) deposition of Ag on a Si(111)-(7x7) substrate at room temperature, Ag was identified under the form of ring-like triangular-shaped atomic structures on top of otherwise undisturbed Si(111)-(7x7) pattern [18]. These ring-like structures constitute the smallest Ag-induced features on the surface and they are interpreted as being the critical nuclei for further Ag condensation. The constant current topographies obtained at two different bias voltages (2 V and -2 V) clearly show that tunneling into unoccupied states gives different images from those obtained by tunneling from the occupied states, where the subunit appears as a three-lobe structure pointing into the direction of the inner adatoms of the unit halves. This again demonstrates that atomically resolved protrusions in STM images may not directly be assigned to atoms.

2.2. Modifications of semiconductor surfaces

The STM is increasingly used as a means of producing nanometer-scale surface modifications at the surface of semiconductors or other materials. There are several procedures among which the most simple are: -the mechanical low-load indentation produced by the tip into Si, or GaAs surfaces to obtain triangular shaped protrusions [19]; -the voltage pulses making it possible to obtain the "foot print" of the tip on silicon or various other single or multiple features [20].

More complicated, a novel electrochemical device was used for direct micromachining of a semiconductor substrate by guiding an ultramicroelectrode tip in a predefined pattern above the surface. A high resolution photoelectrochemical etching of GaAs was thus performed with a scanning electrochemical and tunneling microscope [21].

2.3. STM studies on TiO_2

Transition-metal oxides (TiO_2,...) and chalcogenides (CdS,...) are known to be catalytically active for a large number of thermal and photoreduced chemical processes. Surface energetics and surface states play an important role in the efficiency and range of applicability of TiO_2 and other semiconductor materials, but observation on the atomic scale of defects, adsorbates and other features on their surface became possible only by STM and related local probe microscopies.

TiO_2(110) The effect of reduction on the topographic and electronic structure of TiO_2(110) surfaces was investigated in ultrahigh vacuum using STM, STS and LEED [22]. The structures and electronic properties of hydrogen-annealed, vacuum-annealed and ion-sputtered surfaces were compared with those of the stoichiometric surface. Both the hydrogen and vacuum-annealed surfaces exhibited significant spatial inhomogeneity on the nanometer scale. The observed surface defect structures resulting from different reduction sequences are associated with the reduction mechanisms.

Atomic-resolved images were obtained for a reduced TiO_2(110) surface in UHV [23]. Structural units with periodicities ranging from 2.1 to 3.4 Å have been clearly imaged and the surface structures were explained by a model involving ordered arrangements of two-dimensional defects known as crystallographic shear planes. Oxygen vacancies formed along the (121) plane can be localized but each Ti atom cannot be clearly imaged.

n-TiO_2(001) Tunneling spectroscopy was performed on single crystal n-TiO_2 (hydrogendoped)(001) substrates in air [24]. Cyclic bias scans have shown consistent hysteresis in tunneling spectra, a phenomenon believed to be a manifestation of tip field-induced intra-gap surface and/or near surface states.

The (001) surface of highly doped n-type TiO_2 crystal was examined in air by STM and STS [25]. High-resolution images showing Ti atoms can be obtained with the sample held at negative voltage. STS curves with the tip over a given spot on the TiO_2 surface show electron tunneling into the conduction band and from the valence band. Surface states can be associated with various defects and chemical contamination.

A short photoelectrochemical etching produces at the surface of a single crystal rutile many flat areas and improves both the maximum photocurrent (an order of

magnitude higher than for unetched surface) and the photocurrent onset potential (shifted 700 mV versus the cathodic limit) of the electrode [26].

Polycristalline TiO_2/Ti: Titanium is a commonly and successfully used biomaterial in dental and orthopaedic applications. The properties of the surface oxide on Ti, namely the surface topography at a level of 1 nm-10 μm influence the favorable tissue response.

Electropolished and thermally oxidized Ti show a smooth surface, with a corrugation of 2-10 nm, while glow-discharged-plasma-treated samples show a highly corrugated surface (≈ 100 nm) [27]. Scanning force microscopy images taken in air of electropolished titanium show that the grain edges are smoother than in the case of titanium evaporated on mica. The hydroxylation of the surface plays an important role in the attachement of adsorbed proteins and thus in the biocompatibility of this material. The oxide film of electropolished Ti behaves as an n-type semiconductor with a band gap extending from 0.5 eV to 0.8 eV [29].

TiO_2/Ti fractal electrodes were prepared as previously described [30] and their morphological features imaged by SFM (Fig. 1a,b).

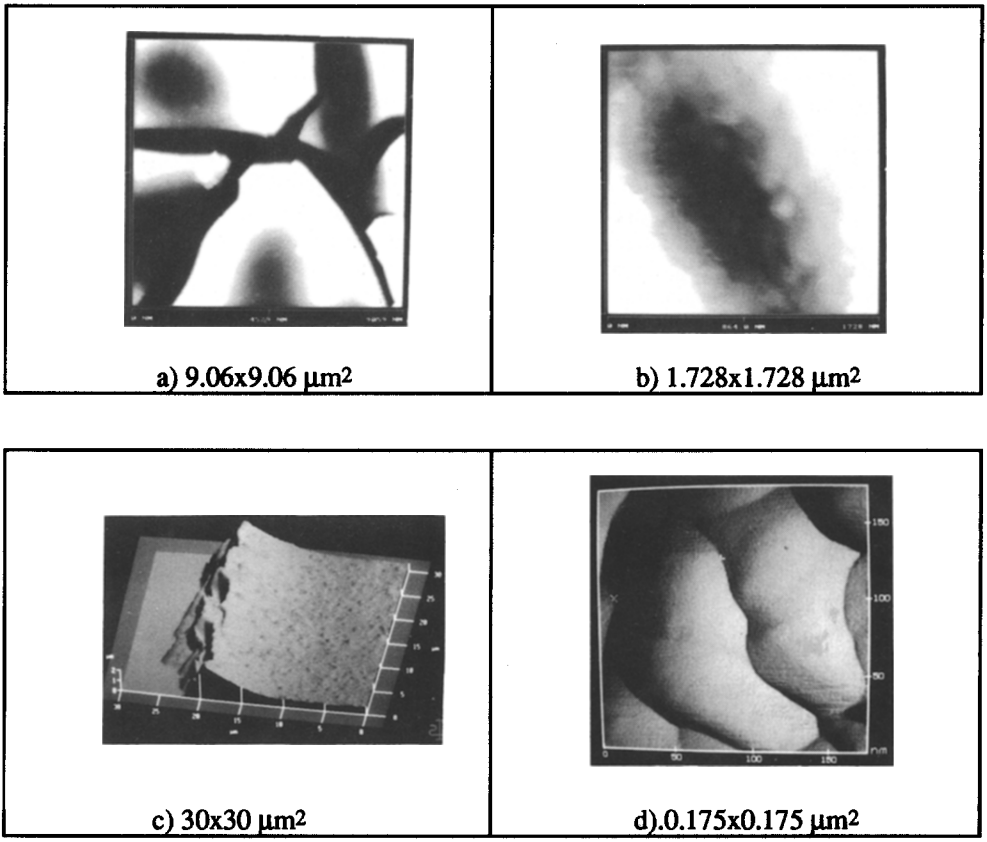

Fig. 1. SFM images of: a,b)fractal TiO_2/Ti electrodes, and; c,d)TiO_2 ceramics.

In addition to the numerous crevices already observed by SEM, small TiO_2 particles, 0.2 μm in size, can be seen on SFM images (Fig. 1b). This make it possible to follow the evolution of these particles during the sol-gel preparation or the thermal treatment.

TiO_2 powders and transparent ceramics: The surface of TiO_2 powder (sieved < 40 mesh ≈500 nm) imaged by STM in air had shown a roughness in a nanometer-scale range [31].

The form of I-V curves obtained by STS showed a stable rectifying behavior of the tunnel function for titanium powder.

Transparent TiO_2 ceramics were prepared from suspensions of a commercial TiO_2 (P25 Degussa) powder deposited as previously described [32] on a conducting glass and subsequently heated at 400 °C. The thickness of the ceramic film imaged by SFM (Fig. 1c) was 1.1 μm, and the size of TiO_2 particles around 0.1 μm (Fig. 1d).

Local probe microscopies (STM or SFM) can be helpful to measure the thickness of the ceramic membranes prepared by different methods and to measure the size of the embedded TiO_2 particles as a function of the thermal treatment.

CONCLUSIONS

Local probe microscopies (STM, SFM) operating in the topographic mode are able to provide useful information on the morphological features of semiconducting materials at the micron scale (thickness of films, size of pores and particles) and at the angström scale (ordered domains, boundaries, etc.). By applying different bias voltages (or forces) when using STM (or SFM) in the spectroscopic mode, the surface states can be localized on the surface of semiconductors. Many applications of local probe microscopies in the characterization and the modification (at nanometer scale) of photovoltaic devices or particulate phoytocatalysts are expected in the very near future.

REFERENCES

1 E. Meyer, R. Wiesendanger, D. Anselmetti, H. R. Hidber, H. J. Guntherodt, F. Levy and H. Berger, J. Vac. Sci. Technol. A 8 (1990) 495
2 J. B. Donnet and E. Custodero. L'actualité Chim. (1992) 157
3 R. Wiesendanger, G. Tarrash, L. Scandella and H. J. Guntherodt, Ultramicroscopy 32 (1990) 291
4 H. Tokumoto, K. Miki, V. Morita, T. Sato, M. Iwatsuki, M. Suzuki and T. Fukuda, Ultramicroscopy 42-44 (1992) 816
5 H. Tanaka, M. Udagawa, M. Itoh, T. Ushiyama, Y. Watanabe, T. Yokotsuka and I. Sumita, Ultramicroscopy 42-44 (1992) 864
6 K. Miki, Y. Morita, H. Tokumoto, T. Sato, M. Iwatsuki, M. Suzuki and T. Fukuda, Ultramicroscopy 42-44 (1992) 851
7 R. Moller, R. Coenen, B. Koscowski and M. Rauscher, Surf. Sci. 217 (1989) 289
8 R. Moller, J. Fraxedas, C. Baur, B. Koslowski and K. Dransfeld, Surf. Sci. 264/270 (1992) 817
9 M. D. Pashley, K. W. Haberern and J. M. Gaines, Surf. Sci. 267 (1992) 153
10 M. D. Pashley and K. W. Haberern, Ultramicroscopy 42-44 (1992) 1281
11 Ph. Ebert, G. Cox, U. Poppe and K. UrbanSurf. Sci. 271 (1992) 587
12 J. J. Boland, Surf. Sci. 261 (1992) 17

13 I. W. Lyo, Ph. Avouris, B. Schubert and R. Hoffman, J. Phys. Chem. 94 (1990) 4400
14 R. Kliese, B. Rottger, D. Badt and H. Neddermeyer, Ultramicroscopy 42-44 (1992) 824
15 Ph. Avouris and D. Cahill, Ultramicroscopy 42-44 (1992) 838
16 M. Udagawa, Y. Umetani, H. Tanaka, M. Itoh, T. Uchiyama, Y. Watanabe, T. Yokotsuka and I. Sumita , Ultramicroscopy 42-44 (1992) 946
17 S. I. Park, J. Nogami and C. GF. Quate, J. Microscopy 152 (1988) 727
18 H. Neddermeyer, Critical Review in Solid State and Materials Science 16 (1990) 309
19 M. R. Castell, M. G. Walls and A. Howie, Ultramicroscopy 42-44 (1992) 1490
20 X. Zheng, J. Hetrik, S. T. Yau and M. H. Nayfeh, Ultramicroscopy 42-44 (1992) 1303
21 C. W. Lin, F. -R. Fan and A. J. Bard, J. Electrochem. Soc. 134 (1987) 1038
22 Q. Zhong, J. M. Vohs and D. A. Bonnell, Surf. Sci. 274 (1992) 35
23 G. S. Rohrer, V. E. Henrich and D. A. Bonnell, Science 250 (1990) 1239
24 S. E. Gilbert and J. H. Kennedy, Surf. Sci. 225 (1990) 21
25 F. R. F. Fan and A. J. Bard, J. Phys. Chem. 94 (1990) 3761
26 S. E. Gilbert and J. H. Kennedy, Electrochem. Soc. 135 (1988) 2385
27 H. Holin, B. O. Aronsson, B. Kasemo, J. Lausmaa and M. Rodahl, Ultramicroscopy 42-44 (1992) 567
28 H. Jobin, M. Taborelli, R. Emch, F. Zenhausern and P. Descouts, Ultramicroscopy 42-44 (1992) 637
29 P. Descouts, R. Emch, M. Jobin and F. Zenhaussern, Proc. 3rd. Int. Symp. on Ceramics in Medecine, Nov 1990
30 N. Neuman-Spallart and O. Enea, J. Electrochem. Soc. 131(1984) 2767
31 B. A. Kwetkus and K. Sattler, Ultramicroscopy 42-44 (1992) 749
32 O. Enea, J. Moser and M. Gratzel, ISE Ext. Abstr. 40-2 (1989) 699.